Volume 1 | Number 1 | Jan 2013 | Pages 1–100

Journal of
Materials Chemistry A

Materials for energy and sustainability
www.rsc.org/materialsA

Li⁺

ROYAL SOCIETY
OF CHEMISTRY

ROYAL SOCIETY
OF CHEMISTRY

www.rsc.org/materialsA

Journal Name

COMMUNICATION

Efficient plasmonic photocatalytic activity on silver-nanoparticle-decorated AgVO$_3$ nanoribbons

ZHAO Wei[#, b], LIANG Feng[#, a], JIN Zhi-Ming[a], SHI Xiao-Bo[a], YIN Peng-Hui[a], WANG Xue-Ren[a], SUN Cheng[*, b], GAO Zhan-Qi[*, b], LIAO Liang-Sheng[*, a]

Ag/AgVO$_3$ plasmonic photocatalyst was synthesized via in-situ reduction of AgVO$_3$ by NaBH$_4$ at room temperature. The Ag/AgVO$_3$ showed high photocatalytic activity due to the relatively high conductivity and electron-storing capacity of Ag nanoparticles, which facilitate the charge transfer between AgVO$_3$ and Ag nanoparticles. FDTD simulation indicates the formed Ag nanoparticles induce SPR leading to increased electric field and the enhanced absorption of visible light.

Silver vanadium oxides nanomaterials (AgVO$_3$, Ag$_3$VO$_4$, and Ag$_4$V$_2$O$_7$, etc.) have attracted extensive attention recently due to their potential applications in rechargeable high-energy density lithium batteries and sensors [1-8]. The unique hybridization of valence bands of V 3d, O 2p, and Ag 4d orbitals in silver vanadium oxides manifests a narrow band gap and highly dispersed valence bands, which could be utilized as visible-light-sensitive photocatalyst [9-11]. As a typical silver vanadium oxides compound, β-AgVO$_3$ has potential application in photocatalysis because of its small band gap and response to visible light. However, the catalytic activity of β-AgVO$_3$ is still low owing to its low capability to separate electron-hole pairs in the photocatalytic reaction, which significantly limits its practical application. Thus, further study is necessary to enhance its photocatalytic performance.

One of the ways to enhance the catalytic activity of a photocatalyst is to construct a system with specific morphology that leads to better performance, as the photocatalytic activity is structure-dependent. Considerable efforts have been made to construct AgVO$_3$ of different morphologies [12, 13]. Among them, one-dimensional nanoribbons having larger aspect ratio for extensive charge separation on their surfaces are expected to be higher activities.

Furthermore, the activity of a photocatalyst would be greatly improved if the photogenerated holes and electrons could be efficiently separated [14–17]. It has been reported that the charge transfer between semiconductor and Ag substantially improves the separation of electrons and holes because Ag has an excellent conductivity and a strong electron-trapping ability [18, 19]. Moreover, Ag modified with nanostructures can induce localized surface plasmon resonance (SPR) [20–22]. The presence of SPR can not only promote the absorption of visible light and the conversion to energetic free electrons, but also increase the rate of electron–hole pair formation due to the electromagnetic field formed near the semiconductor surface [23, 24]. For instance, Huang have developed a series of Ag@AgX (X=Cl, Br, I) plasmonic photocatalysts, which are highly efficient and stable upon visible-light illumination [25, 26]. Lin et al. have reported that the Ag@Ag$_3$(PO$_4$)$_{1-x}$–ZnO hybrid nanoelectrodes exhibit strong photooxidative capabilities which may be attributed to the enhanced near-field amplitudes resulting from localized SPR of Ag–core [27].

On the basis of the above investigations, it seems logical to envision that one of the best ways to fabricate a highly efficient photocatalyst may be to combine these approaches together, that is, one-dimensional AgVO$_3$ nanoribbons and incorporation of silver nanoparticles for SPR generation.

In this communication we report the SPR and the electric field enhancements caused by the Ag nanoparticles as simulated by the three-dimensional finite-difference time-domain (FDTD) method, and the effects of Ag nanoparticles on the electronic and band structure of AgVO$_3$ using the density functional theory (DFT). Furthermore, we describe a facile method to synthesize Ag/AgVO$_3$ plasmonic photocatalysts via an in-situ reduction of AgVO$_3$ nanoribbons by NaBH$_4$ solution

at room temperature. The detailed structural informations and photocatalytic activities of Ag/AgVO₃ plasmonic photocatalysts are investigated and compared with those of corresponding AgVO₃ reference system.

Fig. 1(a) shows the simulative cross-sectional plots of the electric fields of Ag/AgVO₃ nanoribbons by FDTD method. The local ''hot spots'' can be seen in regions between nearly touching Ag nanoparticles [28]. Moreover, the electric field intensity at the AgVO₃ surface is stronger than that of the incident electric field. Thus, the photoabsorption (and hence electron–hole pair generation) rate is expected to be higher than that of the normal incident light [29, 30]. These results strongly suggest that the Ag nanoparticles can facilitate the SPR and the electric field enhancement.

The band structures and density of state calculations of the AgVO₃ and Ag/AgVO₃ plasmonic photocatalysts were carried out via the plane-wave-pseudopotential approach based on density functional theory (Fig. 1(b-c)). The same theoretical model was applied to AgVO₃ (Fig. S2(a)) and the nanostructured Ag/AgVO₃ system (Fig. S2(b)) respectively. From Fig. 1(b), it can be seen that AgVO₃ is a narrow band gap semiconductor with a band gap energy of 2.01 eV. With Ag nanoparticles incorporated on the surface, the band gap of AgVO₃ reduces (1.50 eV, Fig. 1(c)) due to the fact that the Ag 5s orbital by association with Ag nanoparticles moves down the CB after hybridization. These introduced states may play a key role in optical excitation because the resulted narrow band gap could lead to enhanced visible light absorption. Fig. 1(b) and 1(c) also show the projected density of states for AgVO₃ and Ag/AgVO₃ systems, respectively. For the AgVO₃ (Fig. 1(b)), it is clear that the conduction band minimum (CBM) has major contribution from V 3d orbital. Whereas the valence band maximum (VBM) is mainly composed of Ag 4d and O 2p orbitals. Moreover, the extensive hybridization of O atoms with adjacent Ag atoms in the VB means the electrons are difficult to be excited as the extensive overlap of the atomic orbitals increase the electrostatic attraction between the nuclear and electrons. For the Ag/AgVO₃ (Fig. 1(c)) system, the Ag 5s orbital dominates the CBM regions, while the VBM is mainly composed of O 2p and Ag 4d orbitals. Fortunately, the hybridization of O 2p and Ag 4d orbitals of Ag/AgVO₃ system is much weaker than that of the AgVO₃ system on the top of the VB, which is beneficial to the excitation of valence band electrons into the conduction band [31].

Motivated by the aforementioned exciting simulation results, we developed a facile method to synthesize Ag/AgVO₃ plasmonic photocatalyst via an in-situ reduction of AgVO₃ by NaBH₄ solution at room temperature (Fig. S1). The in-situ growth of Ag on AgVO₃ nanoribbon is an important step in achieving the robust bonding between Ag and AgVO₃ nanoribbon, which is essential for the effective charge transfer and separation during photocatalysis.
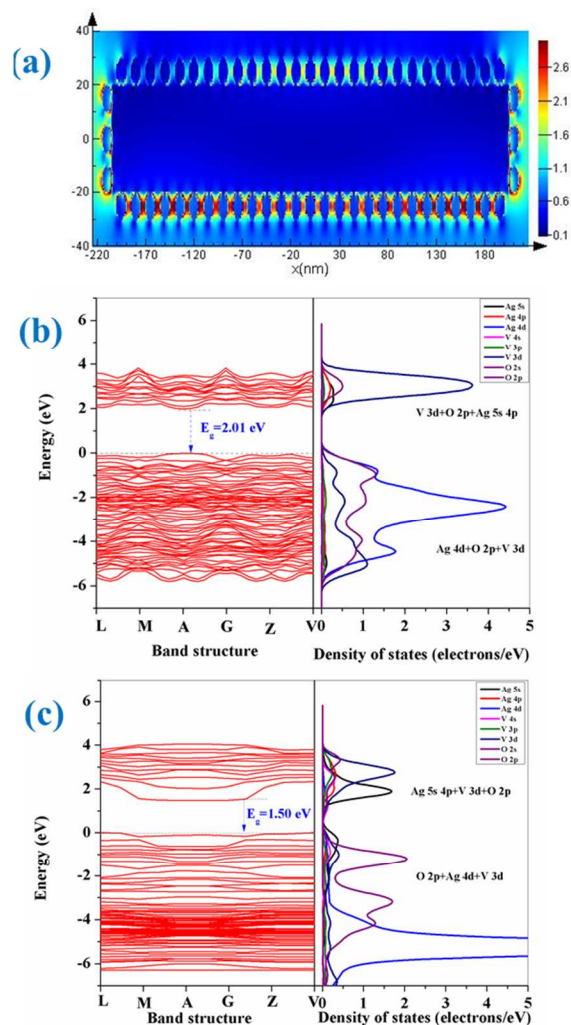

Fig. 1 (a) Electric field distributions calculated at the interfaces of Ag/AgVO₃ using the FDTD method (The thickness and width of simulative AgVO₃ nanoribbon are 50 nm and 400 nm, respectively), calculated band structures and projected density of states of (b) AgVO₃ and (c) Ag/AgVO₃.

XRD and XPS were used to determine the phase structures and the chemical states of Ag species of the as-prepared samples. The XRD pattern of the prepared Ag/AgVO₃ is shown in Fig. 2a along with the pure phase of β-AgVO₃ monoclinic structure [JCPDS: 29-11541] for comparison. The strongest peak (501) indicates the possible preferential orientation of the AgVO₃ nanoribbon [8]. The XRD pattern also indicates that the sample is well crystallized and the crystal phase of AgVO₃ does not change with the decorated Ag nanoparticles on the AgVO₃ surface. The XPS spectra were used to verify the existence of Ag. From the high resolution scanning XPS spectra of the Ag/AgVO₃ (Fig. S3), the two peaks at approximately 368.3 and 374.3eV can be assigned to the binding energies of Ag 3d5/2 and Ag 3d3/2, respectively. The two peaks can be further deconvoluted into four bands (368.1, 368.6, 374.1, and 374.7 eV), implying the presence of different valences of silver species. The two strong peaks at 368.1 and 374.1 eV are

attributed to Ag^+ 3d5/2 and 3d3/2, respectively. Those relatively weak peaks at 368.6 and 374.7 eV match well with that for Ag^o 3d5/2 and 3d3/2, respectively. This is consistent with a previous study reported by Zhu et al. [32]. From the above one can see that two different Ag species exist on the surface of the sample, that is, Ag^+ from the $AgVO_3$ nanoribbons and Ag^o from the Ag nanoparticles. It certainly confirms the presence of Ag nanoparticles on the surface of the sample. Importantly, the surface metallic Ag^o content (mole ratio of Ag^o to Ag^o and Ag^+) was semiquantitatively estimated to be 0.329 by the XPS Ag 3d peak area analysis.

The morphologies of the as-synthesized $AgVO_3$ and $Ag/AgVO_3$ samples were examined by the field emission scanning electron microscope (FESEM), with overview shown in Fig. S4(a). The $AgVO_3$ nanoribbons are about 50-100 nm thick and 100-500 nm wide. Fig. 2(b) shows a single $Ag/AgVO_3$ nanoribbon with numerous Ag nanoparticles of about 10-20 nm in diameter coated on the surface. Further details of morphology were provided from the HRTEM image in Fig. 2(c), where the interplanar distances are determined to be 0.238 and 0.306 nm, which are in accordance with the d-spacings of the (111) crystal plane of Ag and (501) crystal plane of $AgVO_3$ respectively [33, 34], confirming the co-existences of $AgVO_3$ and Ag in the hybrid nanoribbons.
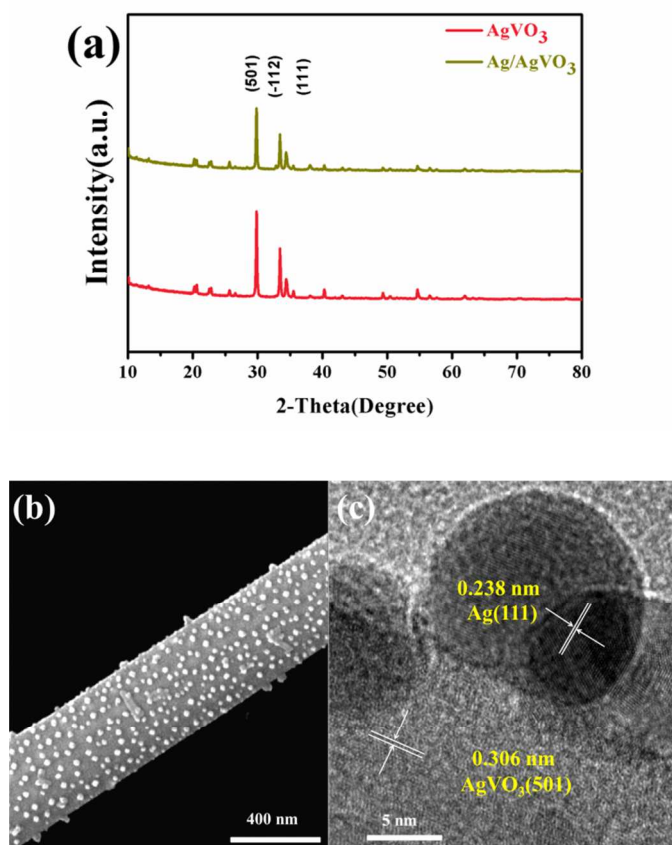

Fig. 2 (a) XRD patterns of the as-prepared samples. (b) FESEM images of the $Ag/AgVO_3$. (c) HRTEM image of $Ag/AgVO_3$.

In order to investigate the optical property changes caused by the incorporation of Ag nanoparticles, fluorescence emission spectra and UV–vis absorption spectra were measured. As shown in Fig. 3(a), the $AgVO_3$ is relatively strongly emissive, indicating that electrons and holes of $AgVO_3$ are easy to recombine. The relative intensity of $Ag/AgVO_3$ is lower than that of $AgVO_3$, implying that the Ag nanoparticles formed on the surface of the $AgVO_3$ nanoribbon are helpful in suppressing the recombination of electrons and holes, which is attributed to the efficient charge transfer between Ag and $AgVO_3$. Photocurrent measurements were also carried out to evaluate the capacity of photogenerated charge separation. The $Ag/AgVO_3$ displayed a much enhanced photocurrent density of 1.7 uA cm^{-2}, about 3 times that of $AgVO_3$ (Fig. 3(b)). UV–vis absorption spectra of the two systems are shown in Fig. 3(c). Interestingly, compared with $AgVO_3$, the $Ag/AgVO_3$ exhibits broad absorption in the whole visible region with higher intensity, which should be attributed to the SPR effect of the Ag nanoparticles formed on the surfaces. Obviously, the Ag nanoparticles could remarkably enhance the absorption of light. Therefore, the formation rate of electron-hole pairs on the $Ag/AgVO_3$ sample surface/interfaces may also increase, resulting in a better photocatalytic performance. In addition, the band gap energy (E_g) of the $AgVO_3$ could be calculated by the equation $(\alpha h\nu)^n = A (h\nu-E_g)$, where α, h, ν, E_g, and A are the absorption coefficient, Planck's constant, light frequency, band gap and a constant, respectively. The value of the index n depends on the electronic transition of the semiconductor ($n_{direct}=2$; $n_{indirect}=0.5$), as for $AgVO_3$, n is 0.5. The band gap energy of the $AgVO_3$ can be estimated from the intercept of the tangent to the plot of $(Ah\nu)^2$ vs energy (hν), and was found to be about 2.0 eV, which is good agreement with the previous band structures calculation based on DFT.

In order to further investigate the SPR induced by the formed Ag nanoparticles, the Raman spectra were carried out (Fig. S5). $Ag/AgVO_3$ manifested higher band intensity than that of $AgVO_3$, which could be due to the effects of surface-enhanced Raman scattering [35-37]. Such enhanced Raman scattering could be related to SPR field induced by Ag nanoparticles on $Ag/AgVO_3$ nanoribbon surfaces.

The photocatalytic activities of the samples were evaluated by comparing degradation rates of crystal violet (CV) under visible light irradiation. The degradation of CV is a pseudo-first-order reaction and its kinetics can be expressed as ln $(C/C_0) = k_{app} t$, where C is the concentration of the CV at time t, C_0 is the initial concentration of the CV solution, and the k is the apparent reaction rate constant. As shown in Fig. 4(a), the k_{app} of $Ag/AgVO_3$ (0.01634 min^{-1}) system is found to be about 4 times higher than that of the pure $AgVO_3$ (0.00462 min^{-1}) system. The lifetime of the photocatalyst is also an important parameter for the catalytic process. We studied the stability and the reusability of the $Ag/AgVO_3$ catalyst during CV degradation. The photocatalytic process was repeated four times. As shown in Fig. 4(b), the sample exhibits adequate stability.
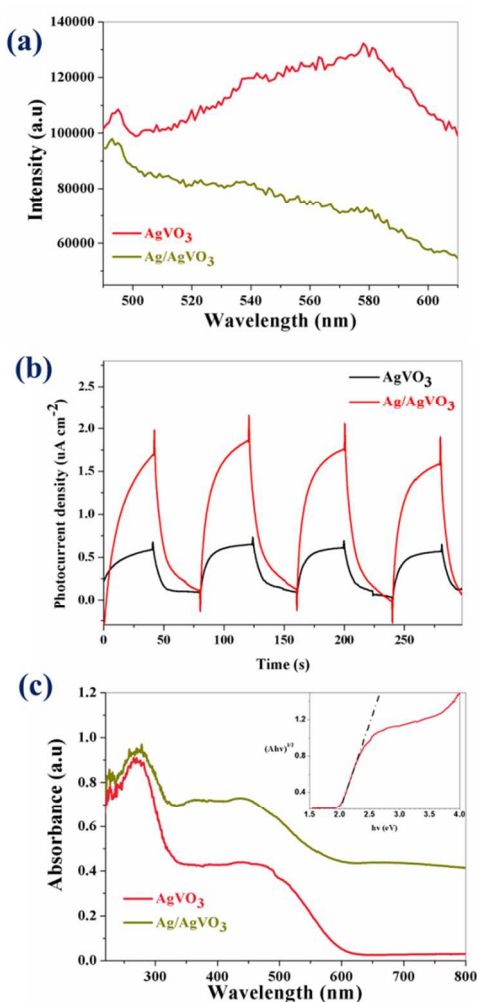
Fig. 3 (a) Room-temperature fluorescence emission spectra of as-prepared $AgVO_3$ and $Ag/AgVO_3$. (b) Photocurrent of $AgVO_3$ and $Ag/AgVO_3$ under visible light irradiation. (c) UV-vis absorption spectra of $AgVO_3$ and $Ag/AgVO_3$ (The inset shows plot of $(Ahv)^2$ vs energy hv).

From the aforementioned observations, we suggest the Ag nanoparticles formed on the ribbon surface play a critical role on the property of the photocatalyst. It is proposed that the strong localized SPR of Ag nanoparticles will remarkably enhance the absorbance of the samples. Therefore, the rate of electron-hole pairs formation in the sample increases substantially. In addition, Ag nanoparticles are also excited due to the localized SPR and generate electron-hole pairs, it means that there are more photogenerated electrons and holes participating in the photocatalytic reaction [38, 39]. Both contribute to the improved activity of the catalyst. Thirdly, Ag nanoparticles could act as electron traps thereby promoting interfacial electron transfer process and enhancing the charge separation of photogenerated electron–hole pairs. This improves the stability of $Ag/AgVO_3$ hybrids by keeping the photoexcited electrons away from $AgVO_3$. Similar suggestions were proposed on Ag_2O [40] and Ag_3PO_4 [41] photocatalysts. Those results strongly confirmed that the structure stability of

Ag-based materials can be remarkably enhanced by Ag nanoparticles. Moreover, the photogenerated electrons trapped by Ag nanoparticles move and accumulate on the surface of Ag nanoparticles and also enhance localized SPR.
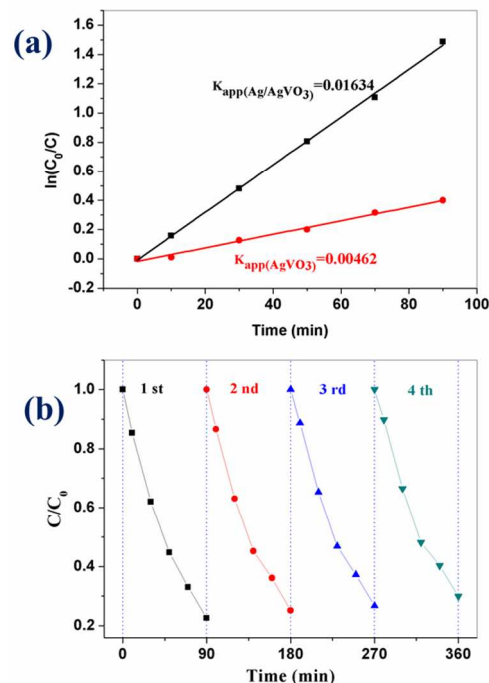

Fig. 4 (a) Pseudo-first-order kinetics of as-prepared photocatalysts for CV degradations. (b) Four recycling runs of $Ag/AgVO_3$ for CV degradations.

As we all know, decompositions of dyes are oxidative processes in which several reactive intermediate species may be involved such as h^+, $\cdot O_2^-$ and $\cdot OH$ [42-45]. To elucidate the reaction mechanism, different scavenges of ammonium oxalate (AO, h^+ quencher), benzoquinone (BQ, $\cdot O_2^-$ quencher) and isopropanol (IPA, $\cdot OH$ quencher) were introduced in the process of CV degradation. As shown in Fig. 5, when an $\cdot OH$ scavenger IPA is added, the k_{app} is slightly reduced. This result indicates that $\cdot OH$ is not the main reactive species in the photocatalytic oxidation process. However, upon the addition of AO and BQ, the k_{app} decrease, suggesting that h^+ and $\cdot O_2^-$ are the main reactive species.
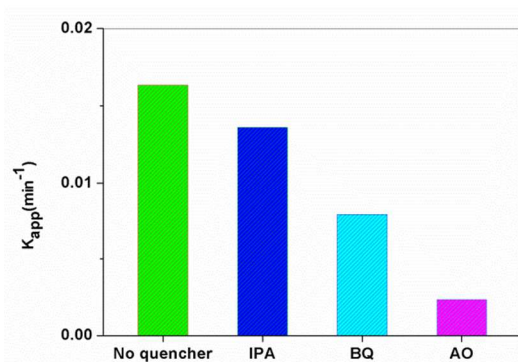

Fig. 5 k_{app} values of $Ag/AgVO_3$ plasmonic photocatalyst with selected quenchers.

Furthermore, the photocatalytic property of the photocatalyst is associated with its band structure. The E_{CB} value of $AgVO_3$ was calculated to be 0.61 eV, and the E_{VB} value was estimated to be 2.11 eV (as shown in our Supporting Information).

Based on the experimental results, the possible mechanism of the $Ag/AgVO_3$ plasmonic photocatalyst under the visible light irradiation is proposed. When the $Ag/AgVO_3$ photocatalyst was subjected to the visible light irradiation, $AgVO_3$ was excited to produce photogenerated electrons and holes. The produced electrons in the conduction band of the $AgVO_3$ would transfer quickly to the Ag nanoparticles, resulting in reduced recombination probability of the formed elections and holes. Moreover, excess electrons would move away from the $AgVO_3$, which diminishes the reduction of Ag^+, leading to more stable $Ag/AgVO_3$ photocatalyst. The more and stable photogenerated holes could oxidize the dye molecules directly on $AgVO_3$ surfaces, which is consistent with the fact that AO demonstrated as the most efficient scavenger to inhibit the oxidative reaction by consuming the formed holes. The photogenerated electrons in Ag nanopartciles and those transferred from $AgVO_3$ could be trapped by O_2 to form $\cdot O_2^-$ reactive oxygen species [46]. The SPR effect, which is produced by the collective oscillations of electrons on the Ag surface, could induce enhancement of the local inner electromagnetic field [47] as evidenced in the FDTD simulations. The VBM potential of h^+ on $AgVO_3$ surfaces (2.11 eV) is not high enough to oxidize H_2O or OH^- into $\cdot OH$, compared with the standard reduction potential of $\cdot OH/H_2O$ (2.27 eV) or $\cdot OH/OH^-$ (2.38 eV) [48]. Therefore, the photocatalytic degradation of CV could be primarily attributed to reacting with h^+ instead of $\cdot OH$ radicals. In addition, the reduction potential of $O_2/\cdot O_2^-$ is -0.33 eV [49]; the CBM potential of $AgVO_3$ (0.61 eV) is not low enough to reduce O_2 to $\cdot O_2^-$ radicals. The transferred electrons from $AgVO_3$ and the photogenerated electrons in Ag nanoparticles are assumed to reduce O_2 to $\cdot O_2^-$, which further reacts with CV.

Conclusions

In summary, a novel one-dimension $Ag/AgVO_3$ plasmonic photocatalyst was synthesized via in-situ reduction reaction of $AgVO_3$ by $NaBH_4$ at room temperature. The photocatalytic performance of the $Ag/AgVO_3$ was higher than that of $AgVO_3$. The enhanced photocatalytic performance could be attributed to the excellent conductivity and the electron-storing capacity of silver nanoparticles, which facilitate the charge transfer between $AgVO_3$ nanoribbons and Ag nanoparticles. Furthermore, the Ag nanoparticles can induce localized s SPR, leading to the electric field enhancement and greater absorption of visible light. The FDTD simulation confirmed that the SPR and the electric field enhancement caused by the Ag nanoparticles. The theoretical calculation based on DFT indicates that Ag formed could narrow the band gap of $AgVO_3$. Meanwhile, the hybridization of O 2p and Ag 4d orbitals of $Ag/AgVO_3$ is weak, which facilitates transfer of valence band electrons into the conduction band. The present study will benefit the development of the other novel Ag-based plasmonic photocatalysts to meet the environmental demands in the future.

Notes and references

a Institute of Functional Nano & Soft Materials (FUNSOM) and Collaborative Innovation Center of Suzhou Nano Science and Technology, Soochow University, Suzhou, Jiangsu 215123, China.
b State Key Laboratory of Pollution Control and Resource Reuse, School of the Environment, Nanjing University, Nanjing 210023, China.
*To whom correspondence should be addressed. E-mail: envidean@nju.edu.cn (C. Sun), lsliao@suda.edu.cn (L. S. Liao).
#These authors contributed equally to this work.

1   L. Y. Liang, Y. M. Xu, Y Lei, H. M. Liu, *Nanoscale*, 2014, **6**, 3536-3539.

2   Z. J. Chen, S. K. Gao, R. H. Li, M. D. Wei, K. M. Wei, H. S. Zhou, *Electrochim. Acta.,* 2008, **53,** 8134–8137.

3   L. Y. Liang, H. M. Liu, W. S. Yang, *Nanoscale*, 2013, **5**, 1026-1033.

4   L. Q. Mai, L. Xu, Q. Gao, C. H. Han, B. Hu, Y. Q. Pi, *Nano Lett.,* 2010, **10**, 2604–2608.

5   S. Liang, J. Zhou, X. Zhang, Y. Tang, G. Fang, T. Chen, X. Tan, *CrystEngComm*, 2013，**46,** 9869-9873.

6   Y. Sang, L. Kuai, C. Chen, Z. Fang, B. Geng, *ACS Appl. Mater. Interfaces*, 2014, **7,** 5061-5068.

7   Q. Zhu, W. S. Wang, L. Lin, G. Q. Gao, H. L. Guo, H. Du, A. W. Xu, *The Journal of Physical Chemistry C*, 2013, **117,** 5894-5900.

8   M. R. Parida, C. Vijayan, C. S Rout, C. S. Sandeep, R. Philip, *Applied Physics Letters*, 2012, **100,** 121119.

9   H. Xu, H. M. Li, L. Xu, C.D. Wu, G. S. Sun, Y. G. Xu, J. Y. Chu, *Ind. Eng. Chem. Res.,* 2009, **48,** 10771–10778.

10   H. F. Shi, Z. S. Li, J. H. Kou, J. H. Ye, Z. G. Zou, *J. Phys. Chem. C,* 2011, **115,** 145–151.

11   P. Ju, H. Fan, B. L. Zhang, K. Shang, T. Liu, S. Y. Ai, D. Zhang, *Sep. Purif. Technol.,* 2013, **109,** 107–110.

12 S. J. Bao, Q. L. Bao, C. M. Li, T. P. Chen, C. Q. Sun, Z. L. Dong, Y. Gan, J. Zhang, *Small,* 2007, **3,** 1174–1177.

13 J. M. Song, Y. Z. Lin, H. B. Yao, F. J. Fan, X. G. Li, S. H. Yu, *ACS Nano.,* 2009, **3,** 653–660.

14 J. X. Wang, H. Ruan, W. J. Li, D. Z. Li, Y. Hu, J. Chen, Y. Shao, Y. Zheng, *J. Phys. Chem. C,* 2012, **116,** 13935−13943.

15 Y. P. Bi, S. X. Ouyang, J. Y. Cao, J. H. Ye, *Phys. Chem. Chem. Phys.,* 2011, **13,** 10071–10075.

16 Y. J. Wang, R. Shi, J. Lin, Y. F. Zhu, *Energy Environ. Sci.,* 2011, **4,** 2922–2929.

17 Z. J. Chen, Z. H. Guan, M. R. Li, Q. H. Yang, C. Li, *Angew. Chem. Int. Ed.,* 2011, **50,** 4913–4917.

18 J. Ren, W. Z. Wang, S. M. Sun, L. Zhang, J. Chang, *Appl. Catal. B,* 2009, **92,** 50–55.

19 Z. X. Ji, M. N. Ismail, D. M. Callahan Jr., E. Pandowo, Z. H. Cai, T. L. Goodrich, K. S. Ziemer, J. Warzywoda, A. Sacco Jr., *Appl. Catal. B,* 2011, **102,** 323–333.

20 M. Murdoch, G. I. N. Waterhouse, M. A. Nadeem, J. B. Metson, M. A. Keane, R. F. Howe, J. Llorca, H. Idriss, *Nat. Chem.,* 2011, **3,** 489–492.

21 Zhou, X. Zhao, H. J. Liu, J. H. Qu, C. P. Huang, *Sep. Purif. Technol.,* 2011, **77,** 275–282.

22 D. J. Wang, G. L. Xue, Y. Z. Zhen, F. Fu, D. S. Li, *J. Mater. Chem.,* 2012, **22,** 4751–4758.

23 Y. X. Zhao, C. Burda, *Energy Environ. Sci.,* 2012, **5,** 5564–5576.

24 J. Baxter, Z. X. Bian, G. Chen, D. Danielson, M. S. Dresselhaus, A. G. Fedorov, T. S. Fisher, C. W. Jones, E. Maginn, U. Kortshagen, A. Manthiram, A. Nozik, D. R. Rolison, T. Sands, L. Shi, D. Sholl, Y. Y. Wu, *Energy Environ. Sci.,* 2009, **2,** 559–588.

25 P. Wang, B. B. Huang, Q. Zhang, X. Zhang, X. Qin, Y. Dai, J. Zhan, J. Yu, H. Liu, Z. Lou, *Chemistry-A Eur. J.,* 2010, **16,** 10042–10047.

26 P. Wang, B. B. Huang, X. Y. Qin, X. Y. Zhang, Y. Dai , J. Y. Wei, M. H. Whangbo, *Angew. Chem. Int. Ed.,* 2008, **41,** 7931–7933.

27 Y. G. Lin, Y. K. Hsu, Y. C. Chen, S. B. Wang, J. T. Miller, L. C. Chen, K. H. Chen, *Energy Environ. Sci.,* 2012, **5,** 8917–8922.

28 W. B. Hou, Z. W. Liu, P. Pavaskar, W. H. Hung, S. B. Cronin, *J. Catal.,* 2011, **277,** 149–153.

29 H. Choi, S. J. Ko, Y. Choi, P. Joo, T. Kim, B. R. Lee, J. W. Jung, H. J. Choi, M. Cha, J. R. Jeong, I. W. Hwang, M. H. Song, B. S. Kim, J. Y. Kim, *Nat. Photonics,* 2013, **7,** 732–738.

30 Z. W. Liu, W. B. Hou, P. Pavaskar, M. Aykol, S. B. Cronin, *Nano Lett.,* 2011, **11,** 1111–1116.

31 S. M. Wang, D. L. Li, C. Sun, S. G. Yang, Y. Guan, H. He, *Appl. Catal., B,* 2014, **144,** 885–892.

32 Q. Zhu, W. S. Wang, L. Lin, G. Q. Gao, H. L. Guo, H. Du, A.W. Xu, *J. Phys. Chem. C,* 2013, **117,** 5894.

33 S. Q. Liang, J. Zhou, X. L. Zhang, Y. Tang, G. Z. Fang, T. Chen, X. P. Tan, *Crystengcomm,* 2013, **15,** 9869–9873.

34 M. W. Shao, L. Lu, H. Wang, S. Wang, M. L. Zhang, D. D. D. Ma, S. T. Lee, *Chem. Commun.,* 2008, **23,** 2310–2312.

35 L. Tong, Z. Li, T. Zhu, H. Xu, Z. Liu, J. Phys. Chem. C, 112 (2008) 7119-7123.

36 Y. Kim, H. Na, Y. W. Lee, H. Jang, S. W. Han, D. Min, Chem. Commun., 46 (2010) 3185-3187.

37 H. Zhang, X. F. Fan, X. Quan, S. Chen, H. T. Yu, Environ. Sci.Technol., 45 (2011) 5731-5736.

38 J. Jiang, L. Z. Zhan, *Chem. Eur. J.,* 2011, **17,** 3710–3717.

39 L. Kuai, B. Y. Geng, X. T. Chen, Y. Y. Zhao, Y. C. Luo, *Langmuir,* 2010, **26,** 18723–18727.

40 X. Wang, S. Li, H. Yu, J. Yu, S. Liu, *Chem.: Eur. J.,* 2011, **17,** 7777–7780.

41 Y. P. Liu, L. Fang, H. D. Lu, L. J. Liu, H. Wang, C. Z. Hu, *Catal. Commun.,* 2012, **17,** 200–204.

42 X. F. Zhou, C. Hu, X. X. Hu, T. W. Peng, J. H. Qu, *J. Phys. Chem. C,* 2010, **114,** 2746.

43 Y. Q. Yang, G. K. Zhang, S. J. Yu, X. Sheng, *Chem. Eng. J.,* 2010, **162,** 171.

44 Y. Y. Li, J. S. Wang, H. C. Yao, L. Y. Dang, Z. J. Li, *J. Mol. Catal. A: Chem.,* 2011, **334,** 116.

45 X. Yang, H. Cui, Y. Li, J. Qin, R. Zhang, H. Tang, *ACS Catalysis,* 2013. **3**, 363-369.

46 J. G. Yu, J. F. Xiong, B. Cheng, S. W. Liu, *Appl. Catal., B,* 2005, **60,** 211.

47 Y. P. Liu, L Fang, H.D. Lu, Y. W. Li, C. Z. Hua, H. G. Yu, *Appl. Catal., B,* 2012, **115–116,** 245.

48 H. F. Cheng, B. B. Huang, Y. Dai, X. Y. Qin, X. Y. Zhang, *Langmuir,* 2010, **26,** 6618.

49 J. Kim, C. W. Lee, W. Choi, *Environ. Sci. Technol.,* 2010, **44,** 6849.